Construction and Building Materials 306 (2021) 124879

Contents lists available at ScienceDirect

Construction and Building Materials

journal homepage: www.elsevier.com/locate/conbuildmat

Post-fatigue properties of high-strength concrete subjected to coupled 3D fatigue-static loading

Fujian Yang [a,b], Dawei Hu [a,b,*], Hui Zhou [a,b], Mao Teng [c], Meili Lan [c], Qi Teng [c]

[a] State Key Laboratory of Geomechanics and Geotechnical Engineering, Institute of Rock and Soil Mechanics, Chinese Academy of Sciences, Wuhan 430071, China
[b] University of Chinese Academy of Sciences, Beijing 100049, China
[c] Petrochina Tarim Oilfield Company, Korla 841000, China

ARTICLE INFO

Keywords:
Post-fatigue characteristics
High-strength concrete
Coupled 3D fatigue-static loading
Physico-mechanical properties
Fatigue damage model
Empirical prediction model

ABSTRACT

Concrete structures suffer some damage yet not failed under fatigue load, and then continue to bear 3D redistributed stress. For this, the 3D fatigue loading considering various fatigue factors (e.g. confining stress, axial static stress (ASS) and force amplitude (FA), frequency, and cycle number) is first carried out, and then the 3D static loading is performed. The post-fatigue characteristics of high-strength concrete (e.g. P-wave velocity, S-wave velocity, porosity, gas permeability, triaxial compression strength, and elastic modulus) are gained. The results indicate that 3D fatigue loading weakens mechanical properties, delays wave propagation, and increases seepage paths. An obvious stress threshold is exhibited with increasing axial static stress and force amplitude, that is 80% triaxial compressive strength, where the physico-mechanical characteristics are rapidly weakened due to the energy dissipation caused by crack growth rises increasingly. Compared with 1D fatigue loading, the frequency turning point of weakening effect from decreasing to increasing is advanced under 3D fatigue loading due to the application of 3D stress exacerbates the heat accumulation and creep damage generation. Interestingly, the fatigue damage is likely to be more sensitive to axial load compared to confining stress during 3D fatigue loading. In other words, the promotion effect of axial fatigue load on damage is larger than the restriction of confining stress. Furthermore, the fatigue damage models considering various fatigue factors are proposed. Then, the empirical prediction models of this damage variable to mechanical parameters (strength and elastic modulus) and permeability are established to predict the capacity loss caused by fatigue loading in the design of concrete construction. The testing results in this context could facilitate our understanding of post-fatigue characteristics of high-strength concrete subjected to 3D fatigue loading and guide the safe design of concrete construction.

1. Introduction

Concrete materials have been widely used in fields of construction (e.g. housing, bridge, and artificial island) transportation (e.g. highway, railway, and subsea tunnel), and water conservancy (e.g. dam, convey tunnel, and sluice) due to its accessibility, formability, and durability [1]. Therefore, excellent mechanical properties and permeability performance are highly expected for concrete materials in engineering applications. However, concrete structures would be subjected to various fatigue loading (e.g. vehicle loads) during their service life [2,3], where the mechanical properties and permeability performance of concrete materials will be weakened with the accumulation of damage caused by fatigue loading [4,7]. Therefore, it is of great significance to investigate the structural performance deterioration and fatigue behavior of concrete materials under fatigue loading.

Various fatigue loading tests (e.g. cyclic loading and unloading, constant-amplitude fatigue loading, variable amplitude fatigue loading, and discontinuous fatigue loading) were carried out to understand the fatigue behavior of the concrete materials [5–9]. Some distinctive and important observations were obtained from laboratory testing. For example, under fatigue loading, the cyclic strain, the indicator of irreversible fatigue life, cyclic creep, and fatigue range that is higher than

Abbreviations: ASS, Axial Static Stress; PV, P-wave Velocity; HSC, High-Strength Concrete; LF, Loading Frequency; SV, S-wave Velocity; FA, Force Amplitude; TCS, Triaxial Compressive Strength; CN, Cycle Number; EM, Elastic Modulus.

* Corresponding author at: State Key Laboratory of Geomechanics and Geotechnical Engineering, Institute of Rock and Soil Mechanics, Chinese Academy of Sciences, Wuhan 430071, China.
E-mail address: dwhu@whrsm.ac.cn (D. Hu).

https://doi.org/10.1016/j.conbuildmat.2021.124879
Received 26 March 2021; Received in revised form 30 July 2021; Accepted 7 September 2021
Available online 17 September 2021
0950-0618/© 2021 Elsevier Ltd. All rights reserved.

Table 1
The mix proportions for the high strength concrete.

Strength Grade	Cement (kg/m^3)	Slag powder (kg/m^3)	Secondary fly ash (kg/m^3)	Sand (kg/m^3)	Gravel (kg/m^3)	Water reducer (kg/m^3)	Water (kg/m^3)
C50	400	50	30	750	1060	12	100

monotonic state strain, and the accumulated ultimate and plastic strains after each cycle before rupture, are dependent on the applied fatigue loading cycles of the concrete materials [1,7,10–14]. Nucleation, interaction, and multi-microdefects growth are the main causes for the weakening of Young's modulus of elasticity in the fatigue process [15–17], and the mechanical behavior of concrete materials under fatigue loading is governed by microdefects like kinetics of the microstructure of the concrete materials. Moreover, the different parameters such as loading conditions, load frequency, boundary conditions, stress level, matrix composition, and stress ratio affect the fatigue life of concrete materials [18]. In particular, the applied maximum stress and its range have a critical influence on fatigue life, the higher the applied maximum stress and the stress range, the lower their fatigue life [19–23].

In addition, many researchers focus on the quantitative characterization of the fatigue damage evolution of concrete materials during fatigue loading. Three typical approaches could be given that the phenomenological method, the fracture mechanics method, and the continuum damage mechanics method [8]. The phenomenological method requires a mass of high-quality experimental data, the traditional empirical equation between stress or strain and fatigue life (known as S-N curve or ε-N curve) is usually formulated by regression analysis [24–27], but it doesn't give a constitutive law and can't explain damage mechanism in fatigue [28]. The fracture mechanics method was established by recognizing the crack initiation and propagation in concrete materials [29,30], and one of the most extensively used fracture mechanics models is known as Paris's law which is based on the stress intensity factor [31]. In this way, various modified fatigue models based on Paris' law have been proposed to improve its prediction precision [32–35]. The continuum damage theory has also been developed using thermodynamic concepts under the damage mechanics framework [36,37], where some damage variables to characterize the damage of materials were given and then established the corresponding damage evolution equation [8,28]. In general, the fatigue damage evolution obeys a three-stage rule when subjected to fatigue loading, the damage increases fast at first, slows down then, and increases fast again at last until failure [12,38]. Furthermore, an analytical model applicable to variable amplitude fatigue loading was proposed by Keerthana et al. [12], with the unified concepts of damage and fracture mechanics within a thermodynamic framework.

In practice, the concrete structures suffer some damage yet not failed under fatigue loading [39,40]. In this case, the concrete structures are still in a relatively stable state and will be continuously subjected to the in situ or redistributed stress during the service period [17,41]. In other words, the concrete structures continue to bear static loads after the fatigue disturbance under such conditions. Besides, concrete structures are in a 3D stress state in many cases in the field. However, 1D fatigue tests or numerical simulations were mainly used to study the fatigue behavior of concrete in previous studies [8,42–45]. Thus, enough attention should be given to the post-fatigue characteristics of concrete structures under a 3D stress state, especially for their mechanical properties and damage behavior. In particular, concrete structures such as immersed tube tunnels, dams, and tunnel linings exist in wading environments, the permeability of concrete is a key indicator of its durability [46–48]. From the perspective of engineering structure design, it is also an urgent problem to be solved that quantitatively evaluating fatigue loading on the weakening of concrete structure's service performance. For this, the 3D fatigue loading considering various fatigue factors (e.g. confining stress, axial static stress (ASS) and force amplitude (FA), frequency, and cycle number) is first carried out, and then the 3D static loading is performed. The post-fatigue characteristics of concrete materials such as their physico-mechanical properties and permeability behavior are investigated, and the practical, acceptable and quantitative evaluation models of fatigue loading on the weakening of mechanical properties and permeability performance are established.

2. Experimental program

2.1. Test materials

Due to its high strength, strong impermeability, and satisfactory corrosion resistance, high-strength concrete (HSC) is often used as supporting material in fields of the sea-crossing bridge, subsea tunnel, super high-rise building, and airport construction. Thus, the HSC consist of water, cement, secondary fly ash, slag powder, gravel, sand, and admixture was fabricated as the test material, its mix proportions are

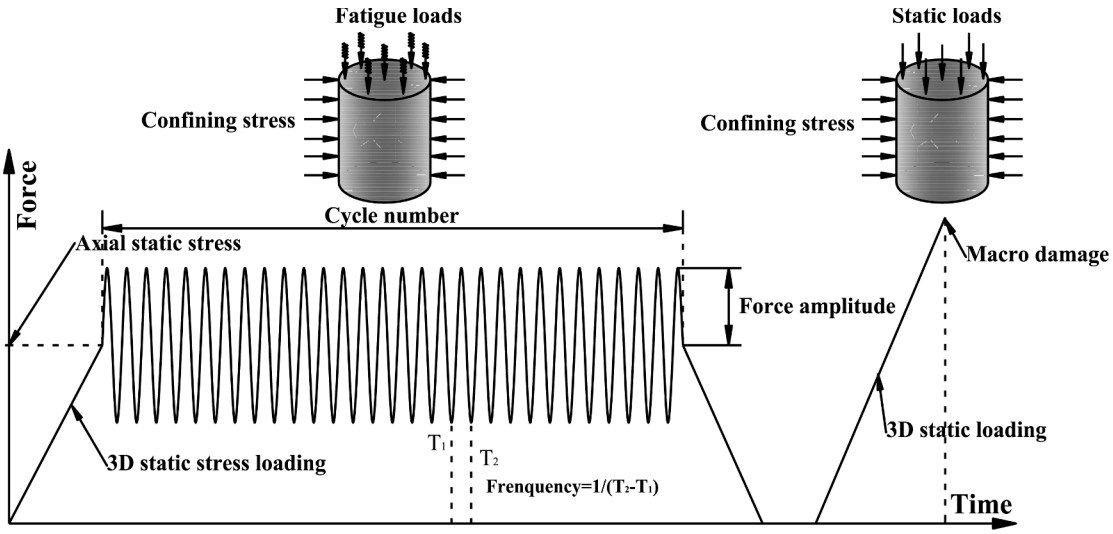

Fig. 1. The stress loading path of the coupled fatigue-static loading (after Yang et al. [17]).

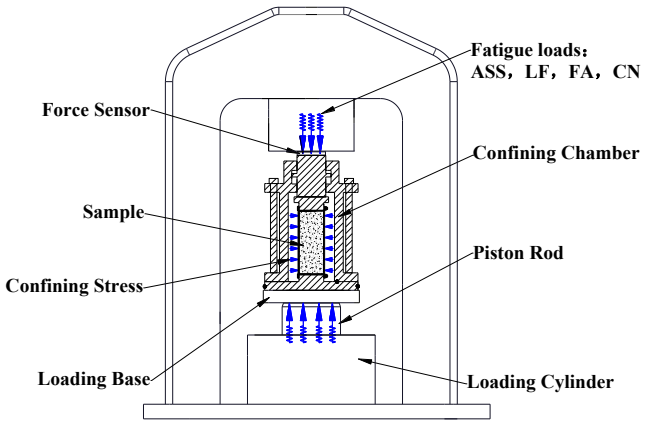

Fig. 2. The schematic diagram of the test system.

Table 2
The uniaxial compressive strengths for the cubic high strength concrete.

Specimens	CUCS-1	CUCS-2	CUCS-3	Average Strength
Uniaxial compression strength	61.56 MPa	65.35 MPa	63.58 MPa	63.50 MPa

shown in Table 1. After a series of processes of uniform mixing of materials, molding, vibrating, and standard curing for 28 d under a constant temperature of 20 ± 2 ℃ and humidity above 95% [49], the cubic concrete specimens with a size of 150 mm × 150 mm × 150 mm were prepared, please Fig. 1. Then, the uniaxial compression tests were performed according to the *Standard for Test and Evaluation of Concrete Compression Strength* (GB50107-2010) [50] for three cubic specimens (CUCS-1, CUCS-2, and CUCS-3), please see Fig. 2, the cubic uniaxial compressive strengths are listed in Table 2.

According to the results of the uniaxial compression tests, the cubic uniaxial compressive strengths are 61.56 MPa, 65.35 MPa, and 63.58 MPa, respectively, all of which meet the standard requirements for HSC according to the *Technical Specification for Strength Testing of High Strength Concrete* (JGJ/T 294-2013) [51].

Standard cylindrical specimens with a diameter of 50 mm and a height of 100 mm were obtained by drilling cubic specimens. A total number of 156 specimens were required for the test, of which 6 specimens were prepared for the measurement of the physico-mechanical properties of the intact concrete specimens under confined conditions, the 6 specimens were used to determine the fatigue life of concrete specimen at the maximum stress level, and the rest were used for the coupled 3D fatigue loading and static loading tests.

2.2. Testing scheme

Firstly, the initial physico-mechanical parameters of the intact concrete specimens were measured as a benchmark, including porosity, permeability, P-wave velocity (PV), S-wave velocity (SV), triaxial compressive strength (TCS), and elastic modulus (EM). Permeability tests and triaxial compression tests were carried out respectively under the different confining stress levels of 2, 5 MPa. The initial physico-mechanical parameters were listed in Table 3, where TCS_i and EM_i mean triaxial compressive strength and elastic modulus of i MPa. Secondly, the coupled 3D fatigue-static loading was performed on the concrete specimens, which includes three steps: axial static loading, fatigue loading, and post-fatigue static loading, as shown in Fig. 1. Then, the parameters, i.e. porosity, permeability, PV, and SV were measured again after the 3D fatigue loading, to analyze the influence of 3D fatigue loading on the concrete fatigue characteristics. Finally, the post-fatigue static loading was conducted to measure the mechanical parameter such as TCS and EM.

2.3. Mechanical testing method

The coupled 3D fatigue-static loading experiment was performed using the triaxial compression dynamic-static test system, which is developed in the Institute of Rock and Soil Mechanics, Chinese Academy of Sciences. The system consists of four major components: loading system, control system, power system, and acquisition system. The maximum axial static load is 1500 kN (the accuracy is 0.01kN), and the frequency can be applied in the range of 0.1 Hz to 10 Hz (the accuracy is 0.1 Hz). The schematic diagram of the test system is shown in Fig. 2.

The static triaxial compression tests were initially performed to determine the mechanical parameter of intact concrete specimens under different confining stress of 2, 5 MPa, as a benchmark for the following 3D fatigue loading tests. The loading rate is 0.12 mm/min and could be considered as quasi-static [52]. The TCS and EM were obtained from three concrete specimens, under different confining stress of 2, 5 MPa.

Five factors were considered in 3D fatigue loading, e.g. confining stress, axial static stress (ASS), fatigue loading frequency (LF), force amplitude (FA), and cycle number (CN). The coupled 3D fatigue loading and static loading tests were divided into two groups based on the confining stress levels (2 MPa and 5 MPa). It is divided into four parts according to fatigue factors (ASS, LF, FA, and CN) in each group. The testing conditions of both groups are listed in Table 4. The LF is mainly in the range of 0.1 Hz to 10 Hz with reference to the work of [17] and [53]. The ASS and AF were comprehensively considered to ensure that the specimen does not undergo macro damage after 3D fatigue loading. Similarly, the maximum CN is determined based on the fatigue life of the concrete at the maximum stress level, that is, the sum of axial static stress plus force amplitude. Three concrete samples were used to determine its fatigue life at the maximum stress level of 95% TCS_5, and the average fatigue life is 6309, please see Table 5. The average fatigue damage evolution is given in Fig. 3, where the fatigue damage was defined by Equation (1). As we can see from Fig. 3, the fatigue damage is divided into three stages, to ensure that the concrete specimen does not undergo macroscopic damage after fatigue loading, the maximum number of cycles is determined to be 5000, that is, $N/N_f = 0.8$.

$$D = 1 - E_f/E_0 \tag{1}$$

where is D the fatigue damage; E_f is the elastic modules during fatigue loading, GPa; E_0 is the initial elastic modulus, GPa.

In addition, as is well known, if a vertical loading is applied, there must be an expansion perpendicular to the loading direction and the confining stress will be altered. For this, the typical curve of change in confining stress with vertical loads variation was given, please see Fig. 4 (a), where the confining stress is kept at a constant in the stage of static loading, whilst it changes with the vertical loading variation in the stage of fatigue loading. Considering the force amplitude of the vertical loading is in the range of 15 ~ 94.50 kN in this paper, the change in confining stress under different force amplitude levels of vertical loading (e.g. FA = 0, FA = 42.00 kN, FA = 63.00 kN, and FA = 94.50 kN) is given

Table 3
Initial physico-mechanical parameters.

Porosity (%)	Permeability ($10^{-18}m^2$)	PV (m/s)	SV (m/s)	TCS_2 (MPa)	EM_2 (GPa)	TCS_5 (MPa)	EM_5 (GPa)
3.21 ~ 3.52	2.40 ~ 2.70	4325.52~4536.22	4675.52~4826.25	77.73~83.59	19.86 ~ 21.52	110.36~114.85	19.02 ~ 21.15

Table 4
Parameters of the coupled 3D fatigue-static loading in group 1 and group 2.

Group No.	Confining stress (MPa)	Axial static stress (kN)	Frequency (Hz)	Cycle number	Force amplitude (kN)	Number of specimens
Group 1	2	45.00 (30% TCS_2)	2.0	1000	30.00 (20% TCS_2)	3
		67.50 (45% TCS_2)				3
		90.00 (60% TCS_2)				3
		97.50 (65% TCS_2)				3
		105.00 (70% TCS_2)				3
		112.5 (75% TCS_2)				3
		90.00 (60% TCS_2)	0.1	1000	30.00 (20% TCS_2)	3
			0.5			3
			1.0			3
			2.0			3
			5.0			3
			10.0			3
		90.00 (60% TCS_2)	2.0	200	30.00 (20% TCS_2)	3
				500		3
				700		3
				1000		3
				2000		3
				5000		3
		75.00 (50% TCS_2)	2.0	1000	15.00 (10% TCS_2)	3
					30.00 (20% TCS_2)	3
					45.00 (30% TCS_2)	3
					52.50 (35% TCS_2)	3
					60.00 (40% TCS_2)	3
					67.50 (45% TCS_2)	3
Group 2	5	63.00 (30% TCS_5)	2.0	1000	42.00 (20% TCS_5)	3
		94.50 (45% TCS_5)				3
		126.00 (60% TCS_5)				3
		136.50 (65% TCS_5)				3
		147.00 (70% TCS_5)				3
		157.50 (75% TCS_5)				3
		126.00 (60% TCS_5)	0.1	1000	42.00 (20% TCS_5)	3
			0.5			3
			1.0			3
			2.0			3
			5.0			3
			10.0			3
		126.00 (60% TCS_5)	2.0	200	42.00 (20% TCS_5)	3
				500		3
				700		3
				1000		3
				2000		3
				5000		3
		105.00 (50% TCS_5)	2.0	1000	21.00 (10% TCS_5)	3
					42.00 (20% TCS_5)	3
					63.00 (30% TCS_5)	3
					73.50 (35% TCS_5)	3
					84.00 (40% TCS_5)	3
					94.50 (45% TCS_5)	3
Total number of specimens						144

Table 5
The fatigue life of the concrete samples at the maximum stress level of 95% TCS_5.

Sample name	Sample A	Sample B	Sampling C
Fatigue life	5467	6540	6920
Average fatigue life		6309	

in Table 6. Interestingly, there is an obvious linear correlation between the change of confining stress and the force amplitude of the vertical load (please see Fig. 4(b)), and the maximum change in confining pressure is only 2.68% (Table 5). Thus, the effect of changes in confining stress caused by the vertical loading variation is not considered in the subsequent experiments. It should be pointed out that the change in confining stress is set to 0 when the force amplitude of vertical load is equal to 0 in Table 6.

2.4. Testing methods of porosity

The concrete specimens were dried to a constant weight using XL101-3 drying oven (accuracy of ± 1 °C) and obtained its weight (M_1) using HZF-A1000 electronic scale (accuracy of ± 0.01 g). The volume (V_1) was calculated based on the external dimensions of the specimens measured using ACE-150 digital vernier caliper (accuracy of ± 0.01 mm). Then, the dried sample was water-saturated using an H15558 vacuum pump (accuracy of ± 0.25%) for 24 h, and the weight (M_2) and

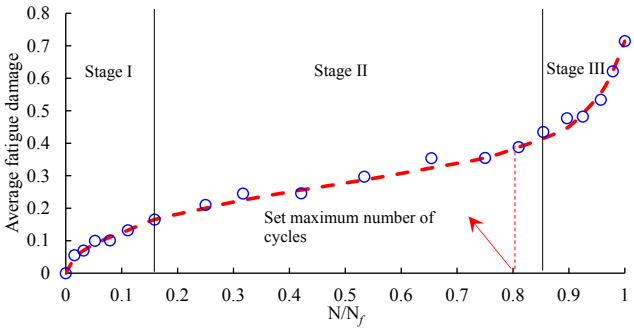

Fig. 3. Average fatigue damage evolution with N/N_f (N_f = 6309).

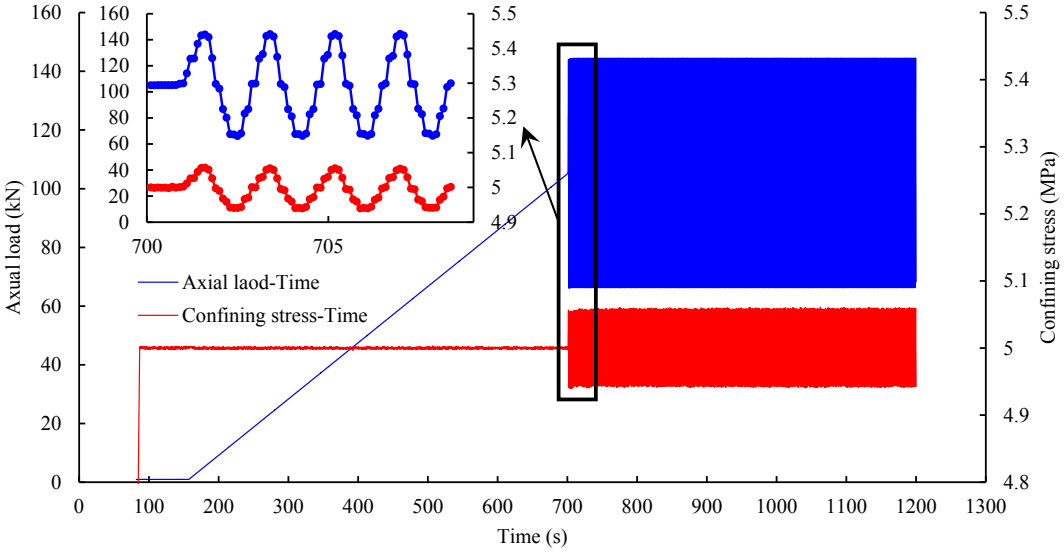

(a) The typical curve of change in confining stress with the vertical loading variation

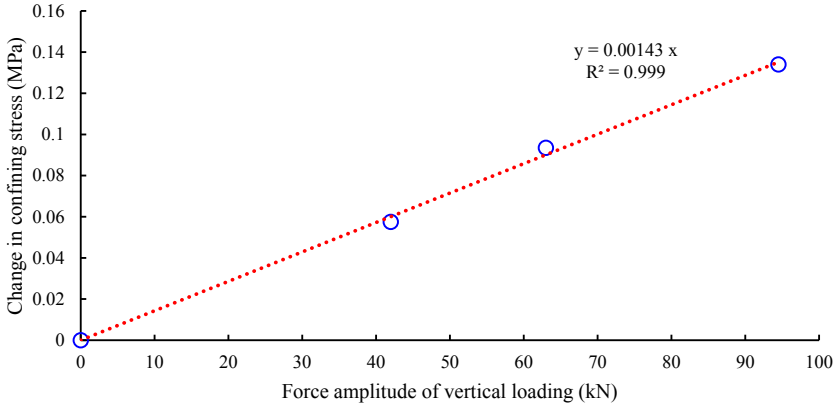

(b) The relationship between the change in confining stress with the force amplitude of vertical loading

Fig. 4. The change in confining stress with vertical loads variation.

Table 6
Change in confining stress with the vertical loading variation.

Confining stress (MPa)	Force amplitude of vertical load (kN)	Change in confining stress (MPa)	Difference (%)
5.0	0.00 (Added)	0.00 (Added)	0.00
5.0	42.00	0.0575	1.15
5.0	63.00	0.0935	1.87
5.0	94.50	0.1340	2.68

the volume (V_2) were measured again for the saturated sample. Therefore, the effective porosity could be calculated by Equation (1).

$$p = (M_2 - M_1)/(V_2\rho w) \times 100\% \quad (1)$$

where p is the effective porosity of the dried sample, %; ρ_w is the density of water, 1.0 g/cm^3.

2.5. Testing methods of ultrasonic wave velocity

PV and SV were measured separately using an RSM-SY5 (N) digital ultrasonic testing device (the accuracy is 0.1 μs). Two types of ultrasonic probes were used, one type for the emission of the P-wave, and the other type for the emission of the S-wave. First, two ultrasonic probes were placed at both ends of the concrete specimen, where the pure water was used as an ultrasound couplant to avoid blocking the seepage channel. Then, the time that the ultrasonic wave propagates in the sample was automatically recorded by the device. The ratios of the sample length to the propagation time were calculated as the PV or the SV of the specimen in the axial direction. Finally, the ultrasonic wave was measured again after the 3D fatigue loading.

2.6. Permeability testing method

The instantaneous pulse method taking Klinkenberg effect into account was used to measure the permeability of concrete specimens due to its characteristics with low-permeability and tightness [54,55], as shown in Equation (2). First, the intact concrete specimens were wrapped in a thermal shrinkable sleeve, then hydrostatic stress equal to 2 MPa was loaded isotropically to avoid gas leakage from the side. Second, a helium gas with stress equal to 1.0 MPa was then injected into the sample at both inlet and outlet, where the sample was uniformly filled with helium gas. Then, the inlet pressure was increased to 1.5 MPa, and a pressure gradient of 0.5 MPa ($\triangle P_0$) was applied between the inlet and outlet. The acquisition system automatically collected pressure change at the inlet and outlet, where the initial permeability was measured based on Equation (2). Finally, the permeability was measured again after the 3D fatigue loading under the same loading condition. The

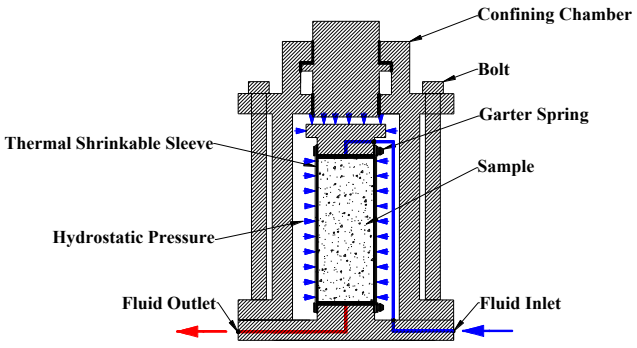

Fig. 5. The schematic diagram of the permeability measurement.

schematic diagram of the permeability measurement is exhibited in Fig. 5.

$$K = \frac{V_1 V_2}{V_1 + V_2} \frac{\beta \mu L}{A \Delta t_i} ln \frac{\Delta P_i}{\Delta P_0} \tag{2}$$

where K is the gas permeability of the specimens; V_1 and V_2 are the volumes of upstream and downstream pressure vessels of 0.45 L and 0.15 L, respectively; where L is the length of the sample; μ and β are the viscosity and compression factor of the gas, their values are 1.89×10^{-5} Pa•s and 0.99 Pa^{-1} in the present study, respectively; A is the cross-sectional area of the specimens; $\triangle T_i$ is the time of the data point calculated from saturation; $\triangle P_i$ is the differential pressure at any time (MPa); $\triangle P_0$ is the initial pressure difference, and $\triangle P_0 = 0.5$ MPa.

3. Results

The post-fatigue characteristics of HSC under the coupled 3D fatigue-static loading were exhibited in this section, including PV, SV, porosity, permeability, TCS, and EM.

3.1. P-wave velocity and S-wave velocity

Figs. 6 and 7 show the variation in PV and SV with fatigue factors (e.g. ASS, LF, FA, and CN) under different confining stress of 2, 5 MPa. The 0.1 ~ 0.85 in the abscissa of Fig. 6(a) and (c) represent 10% ~ 85% of the TCS under the corresponding confining stress. The initial value was measured for each intact concrete sample before the 3D fatigue loading. The results show that the PV and SV after fatigue loading are lower than the initial value, and the reduction is more obvious under higher confining stress (5 MPa). Under the same confining stress level, the PV and SV decrease with ASS, FA, and CN, while a transition from increasing to decreasing is presented with LF.

The experimental results indicate that the fatigue loading weakens the characteristics of wave propagation, and the weakening effect exhibits an enhancement trend with the increase of confining stress. However, the weakening characteristic exhibits different variations for different fatigue factors. Under the low level of ASS (30%, 45%, and 60% TCS_2/TCS_5) and FA (10%, 20%, and 30% TCS_2/TCS_5), the PV and SV show a slow downward trend, with a reduction rate of 0.81 ~ 5.40 m/s·kN, and then a rapid decline is presented with a rate that can be as high as 11.38 ~ 34.00 m/s·kN. Dual characters are exhibited with the increasing of LF, where the PV and SV increase rapidly at a rate of 181.04 ~ 527.90 m/s·Hz in the range of 0.1 Hz ~ 1.0 Hz, and then a slow downward trend is presented with a rate of 11.80 ~ 26.59 m/s·Hz. As for the CN, a typical two-stage downward trend is exhibited, with a reduction rate of 0.19 ~ 0.32 m/s per cycle before 1000 cycles, and then the reduction rate slows to 0.085 ~ 0.091 m/s per cycle.

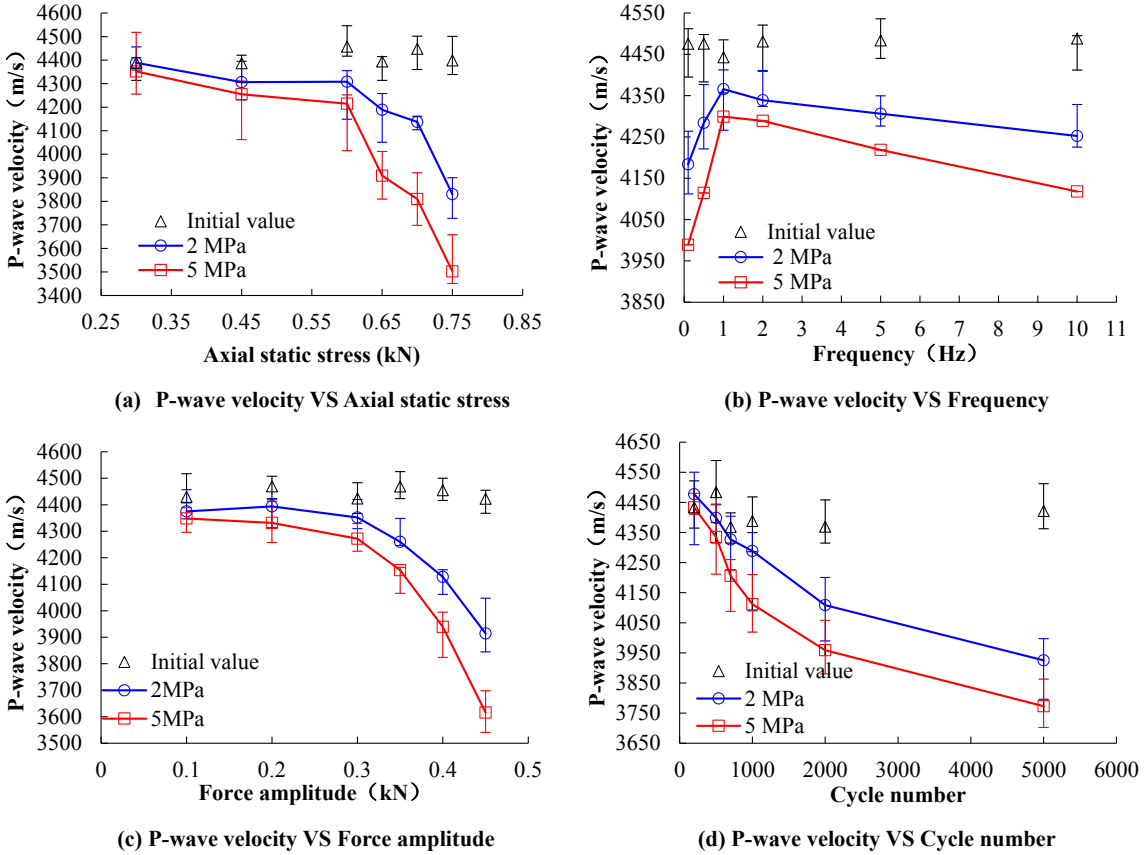

(a) P-wave velocity VS Axial static stress

(b) P-wave velocity VS Frequency

(c) P-wave velocity VS Force amplitude

(d) P-wave velocity VS Cycle number

Fig. 6. Variations in P-wave velocity with fatigue factors under confining stress of 2, 5 MPa.

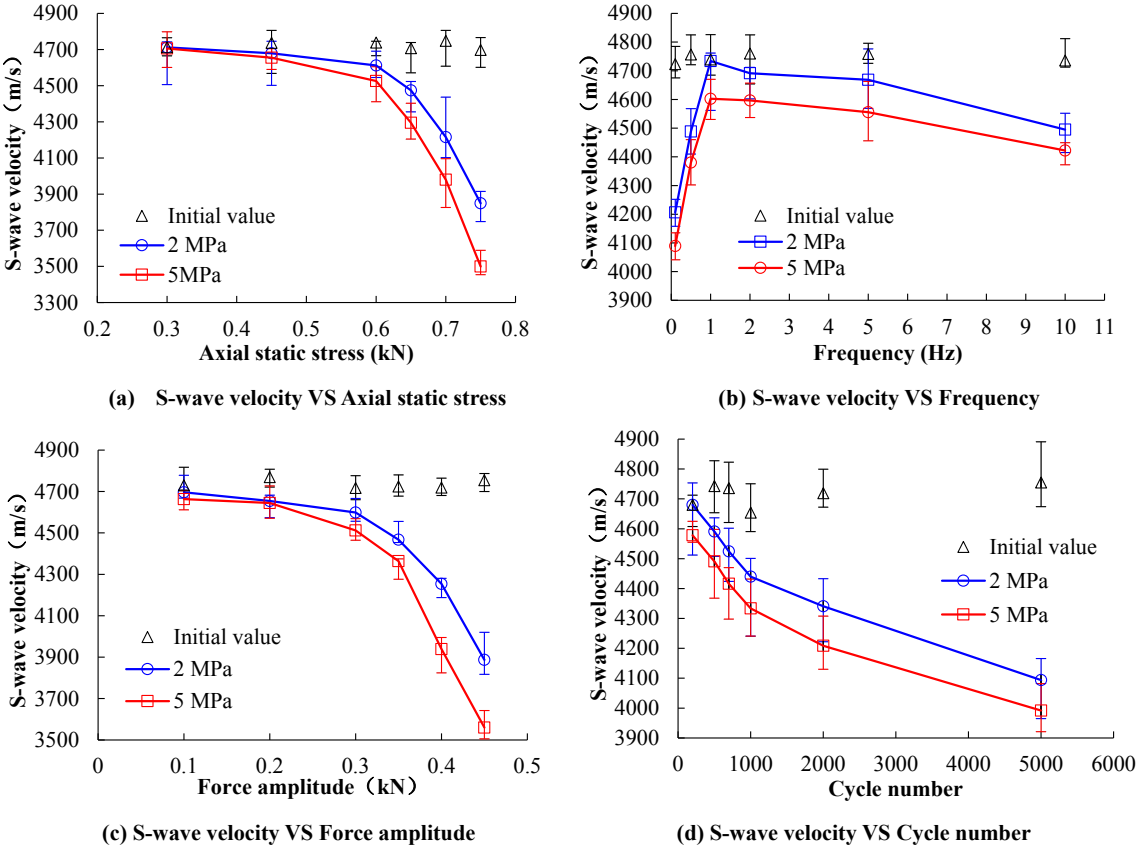

Fig. 7. Variation in S-wave velocity with fatigue factors under confining stress of 2, 5 MPa.

3.2. Porosity and permeability

The variation in porosity and permeability with the various fatigue factors under confining stresses of 2, 5 MPa are exhibited in Figs. 8 and 9. The results indicate that the fatigue loading enhances the seepage capacity, where the porosity and permeability are increased with increasing ASS, FA, and CN, while they undergo a decrease-increase transition with respect to LF. In addition, the enhancement effect is more obvious under confining stress of 5 MPa, which implies that the porosity and permeability have a high sensitivity to the axial loads compared to confining stress.

Similar to PV and SV, the porosity and permeability show different variations with fatigue factors. The porosity and permeability show a slow increment trend under the low level of ASS (30%, 45%, and 60% TCS_2/TCS_5) and FA (10%, 20%, and 30% TCS_2/TCS_5), while they increase rapidly when the stress threshold is exceeded. A noticeable transition from decreasing to increasing is presented with LF for porosity and permeability, and the turning point appears near the frequency of 1.0 Hz. For CN, the porosity and permeability show a two-stage evolution relationship.

3.3. Triaxial compression strength and elastic modulus

Figs. 10 and 11 show the variation in TCS and EM with fatigue factors (ASS, LF, FA, and CN) under confining stresses of 2, 5 MPa. They exhibit similarity with PV and SV, where the mechanical behavior such as TCS and EM were degenerated by fatigue loading, and the weakening was further strengthened under higher confining stress. However, the different variations were presented with fatigue factors. With the increase of ASS, LF, and CN, the TCS and EM were gradually decreased, while the transition characteristics were given for LF from increasing to decreasing. It is interesting that there was an obvious stress threshold for ASS and LF, that is, the maximum axial stress, the sum of the ASS plus FA reaches 80% TCS_2/TCS_5, and they will be decreased rapidly once exceeding the threshold as well as PV and SV.

4. Discussion

4.1. The weakening mechanism of concrete under the coupled 3D fatigue loading and static loading

As we mentioned, the physico-mechanical characteristics of HSC were degraded by fatigue loading, where the parameters such as PV, SV, TCS, and EM are decreased, whilst the permeability and porosity are further increased. The reason for this phenomenon is the non-uniform cracks were propagated inside concrete specimens during fatigue loading, and the cracks propagating along the loading direction are predominant, which has been observed cleanly by Skarzynski et al. [56] using X-ray micro-CT images. Subsequently, the growth of cracks results in the weakening of mechanical properties (TCS and EM), delay of P-wave and S-wave propagation, and increase of the transport paths.

4.2. The weakening mechanism of concrete for ASS and FA

However, it is interesting that the weakening effect exhibits an obvious difference for various fatigue factors. With the increase of the fatigue factors of ASS and FA, the physico-mechanical characteristics of HSC show a slight change under the low level of ASS (30%, 45%, and 60% TCS_2/TCS_5) and FA (10%, 20%, and 30% TCS_2/TCS_5), whilst the weakening effect is significantly strengthened under the high level of ASS (65%, 70% and 75% TCS_2/TCS_5) and FA (35%, 40% and 45% TCS_2/TCS_5). This indicates that there is an obvious stress threshold, the maximum stress level, the sum of the ASS plus FA reaches 80% TCS_2/TCS_5. This could be explained by the cumulative damage caused by

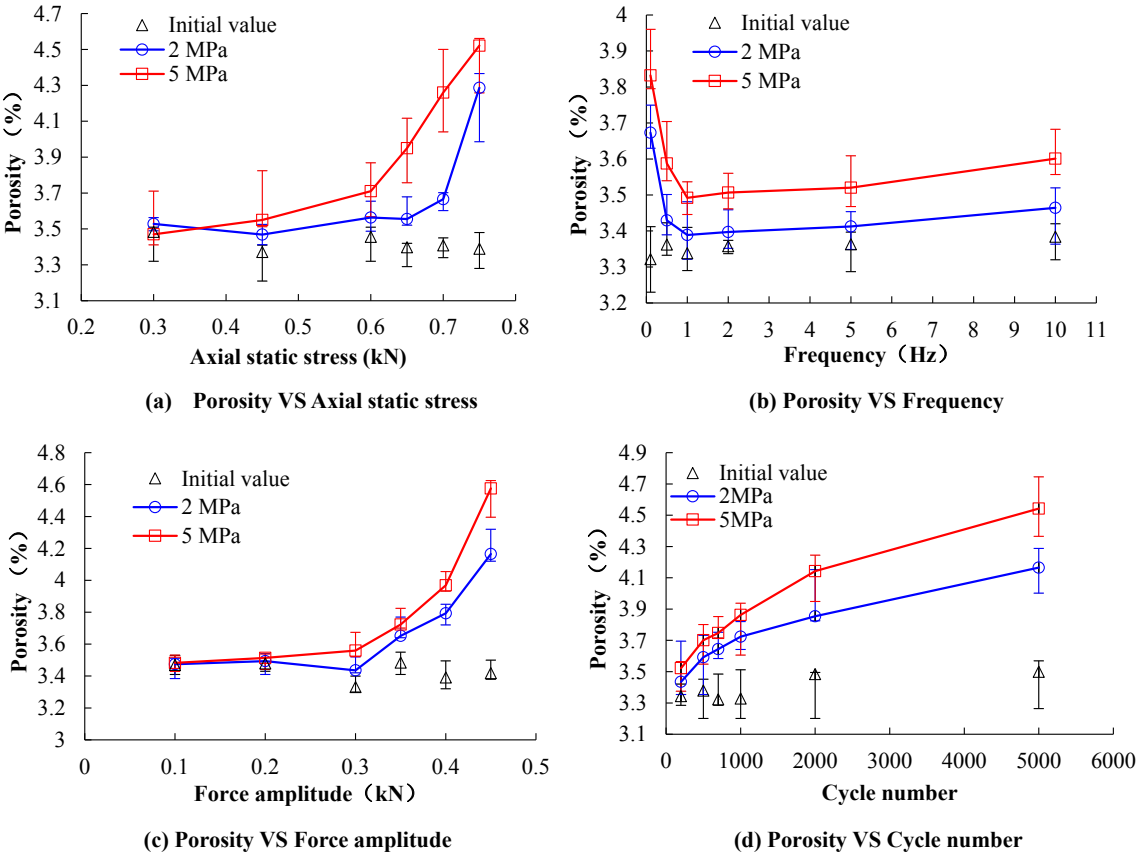

Fig. 8. Variation in porosity with fatigue factors under confining stress of 2, 5 MPa.

energy dissipation. First, the stress level effect on fatigue characteristics of concrete can be ascribed as the damage accumulation rate [57]. Furthermore, the results of Tepfers et al. [58], Lei et al. [59], and Zhang et al. [44] indicated that the energy dissipation caused by crack growth rises increasingly when the stress level exceeds $0.8\sigma_c$, accelerating the development of concrete damage dramatically, please see Fig. 12. Thus, the physico-mechanical characteristics of HSC are rapidly weakened after exceeding the maximum stress level of 80% TCS_2/TCS_5 in this paper.

4.3. The weakening mechanism of concrete for LF

Previous studies [60–62] indicated that the effect of LF on fatigue characteristics of concrete was significant when the maximum stress level was greater than $0.75\sigma_c$, resulting in changes in fatigue life. Thus, the LF has a significant influence on the physico-mechanical characteristics of HSC under the maximum stress level of 80% TCS_2/TCS_5 in this paper. However, a noticeable transition characteristic was exhibited for LF. Firstly, the weakening effect caused by fatigue loading decreases with LF in a range from 0.1 Hz to 1.0 Hz. The loading frequency effect on fatigue characteristic of concrete can be ascribed as the creep damage accumulation in a range from 0.1 Hz to 1.0 Hz [63]. The increment of creep damage is a consequence of the greater duration of tests and consequently the increase of creep damage [56,61]. Thus, the weakening effect caused by fatigue loading is more obvious in lower frequencies. Secondly, the opposite result is presented with a frequency from 1.0 Hz to 10.0 Hz, where the weakening effect increases with frequency. This could also be explained by the self-heating effect caused by frequency loading. The time between cycles is not sufficient to dissipate the heat generated by that friction between the contacting faces of the fissures in high-frequency fatigue tests [64], result in increasing the temperature of the concrete. This exists throughout the fatigue loading and accelerating the creep damage of the concrete, so weakening the physico-mechanical characteristics. A similar experimental phenomenon, the frequency threshold of weakening effect, was observed by Eftekhari et al. [65] and Thomas et al. [63], where the fatigue life at higher frequencies is less than that at lower frequencies when exceeding the frequency threshold. However, it is interesting that, compared with the uniaxial compression fatigue loading, the frequency threshold of weakening effect is advanced for 3D fatigue loading in this paper, from 4.0 Hz ~ 15.0 Hz [63,65] to 1.0 Hz. The reason is that the application of 3D stress limits the lateral deformation of concrete and energy dissipation, thus exacerbating the heat accumulation and creep damage generation.

4.4. The weakening mechanism of concrete for CN

As shown in the results, the weakening effect is in accord with the two-stage damage evolution theories with the increasing number of cycles [26,66,67], where the nonlinear evolution relationship is presented between damage and CN in the low-cycle stage, and then a linear relationship is exhibited for both of them. This could be explained by the damage accumulation caused by crack growth with the increasing number of cycles on the lifetime scale of the corresponding load range [3,68,69]. Firstly, in the low-cycle level, the growth of cracks inside concrete specimen is in the initiation stage with strong randomness [70,71], resulting in a nonlinear damage variation. However, the growth of cracks is in the propagation stage under a high-cycle level [70,71], where new cracks begin to develop and propagate steadily [72–74]. Thus, the damage exhibits a good linear relationship to CN.

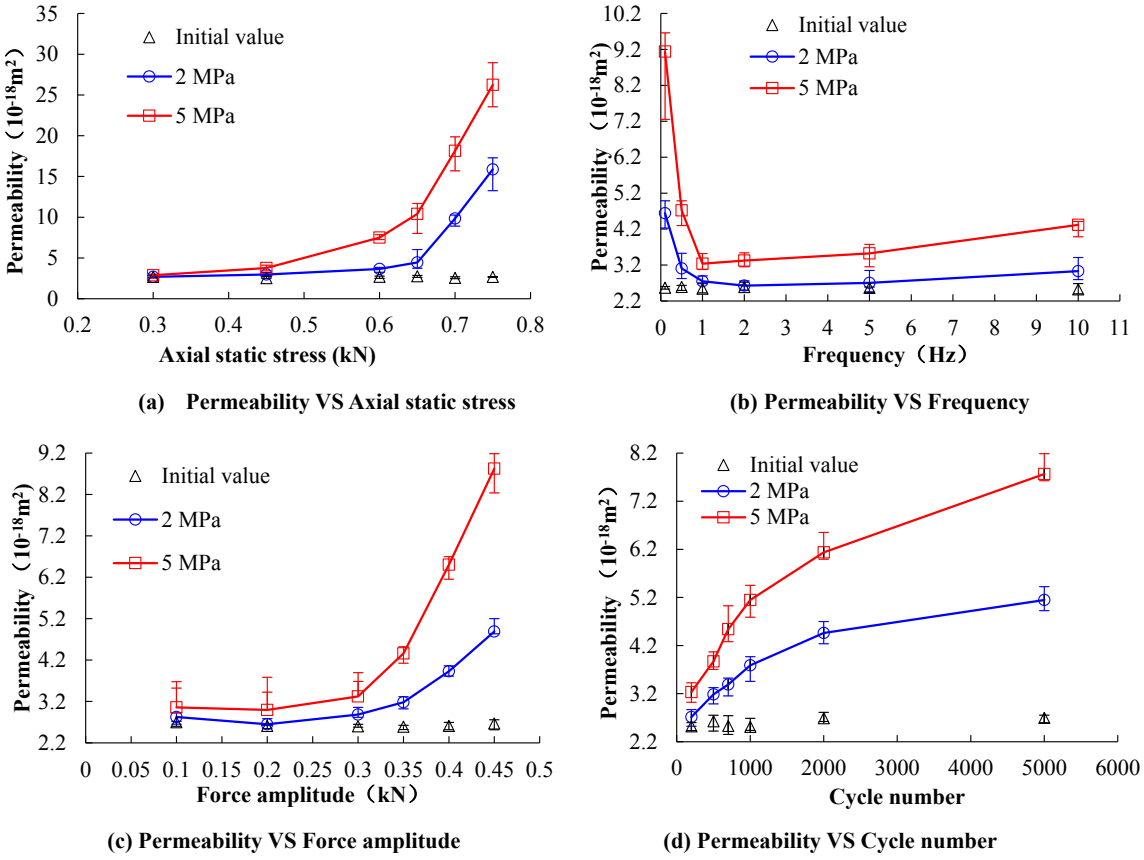

(a) Permeability VS Axial static stress

(b) Permeability VS Frequency

(c) Permeability VS Force amplitude

(d) Permeability VS Cycle number

Fig. 9. Variation in permeability with fatigue factors under confining stress of 2, 5 MPa.

5. Evolution of damage accumulation and establishment of the empirical prediction model

Excellent mechanical properties and permeability performance are highly expected for concrete materials in engineering applications. However, with the change of actual loads caused by various fatigue loading (e.g. traffic loads and seismic loads), the mechanical properties and permeability performance of concrete materials will be deteriorated with the accumulation of damage caused by fatigue loading [1]. Therefore, the determination of mechanical properties and permeability performance of concrete materials subjected to fatigue loading is of great significance. For this, it would be nice to establish a direct relationship between the ASS, LF, FA, and CN of fatigue loading to a damage variable. Then the relationship of this damage variable to mechanical parameters (TCS and EM) and permeability is established. Hence, any designer could incorporate directly a loss of capacity caused by fatigue loading in the design of any concrete construction.

5.1. Damage accumulation caused by fatigue loading

As shown by the experimental results, the mechanical properties and permeability performance of concrete materials are deteriorated due to the accumulation of damage caused by fatigue loading, and the weakening effect exhibits different variations for different fatigue factors (ASS, LF, FA, and CN). Therefore, the direct relationships between the ASS, LF, FA, and CN of fatigue loading to a damage variable need to be established separately. For a pragmatic monitoring purpose, some of the non-destructive variables could be selected, especially those which could be measured in the field. Fortunately, measurement of the ultrasonic wave is comparably an easy and simple task, which can be conducted in site and laboratory to characterize the fatigue properties of materials [75]. Thus, the damage variable can be defined based on the S-wave velocity that is closely related to the elastic constant, density, and development of cracks [76], please see Equation (5). It should be noted that ASS and FA are considered comprehensively as the maximum axial stress (S_{max}), that is, the sum of the ASS plus FA. Here, we further added four available data to the accuracy of the fatigue damage model, please Table 7.

$$D = 1 - V_{sf}^2/V_{s0}^2 \tag{5}$$

where V_{sf} is the SV of the specimens subjected to fatigue loading, m/s; V_{s0} is the SV of the intact specimens, m/s.

Under the current experimental conditions, good correlation relationships are exhibited between damage variable versus ASS, LF, FA, and CN of fatigue loading, as we can see from Fig. 13. The best-fit curves are selected separately, and the fitting equations and correlation coefficients are given in Table 8. It can be inferred that a 'Nike' shape regression relationship is obtained for the damage variable and LF, an exponential regression relationship is exhibited for damage variable and maximum axial stress, and the two-stage damage evolution relationship is given for CN. From these relationships, one could be easily obtained the first prediction of the damage subjected to fatigue loading with different fatigue factors. In addition, it is interesting that the damage caused by fatigue loading under the confining stress of 5 MPa is greater than that of 2 MPa, which indicates that the promotion effect of axial loads on damage is larger than the limiting effect of confining stress. In other words, the damage has a high sensitivity to the axial loads compared to confining stress. Meanwhile, this can also explain why the weakening effect is enhanced at high confining stress levels as shown in experimental results.

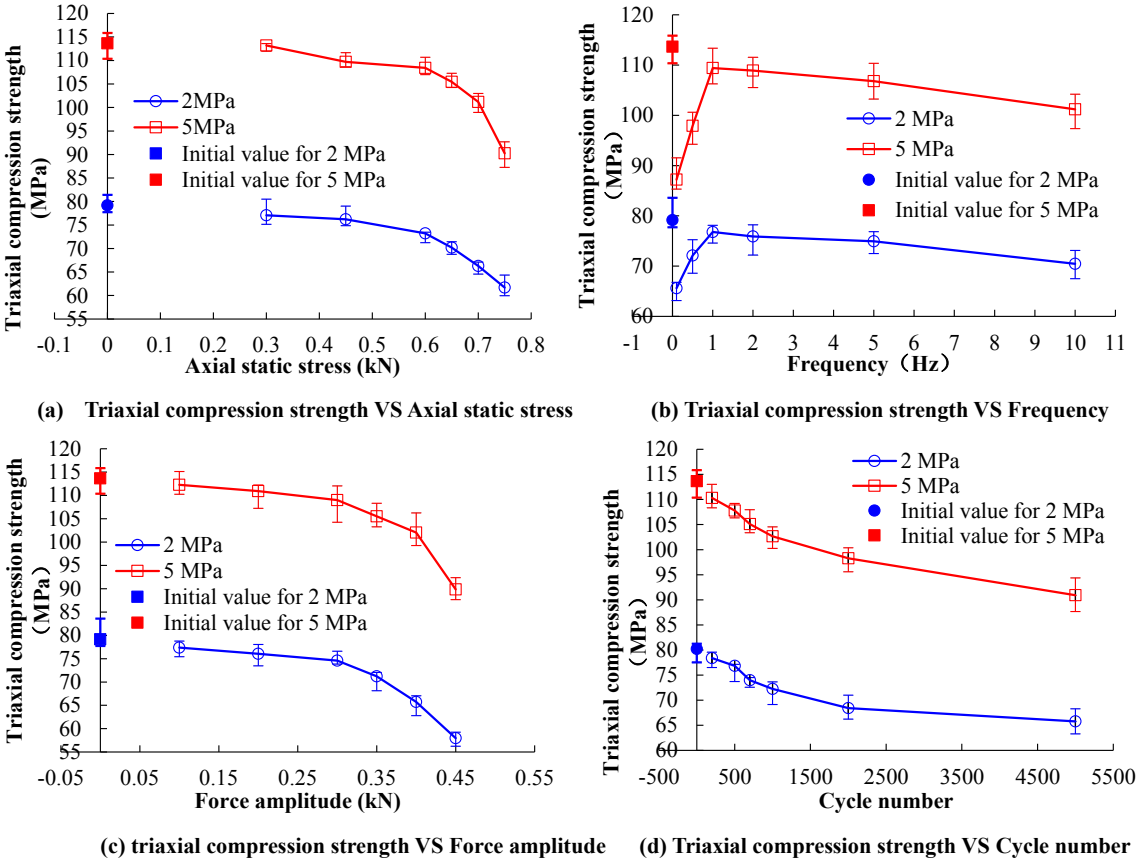

Fig. 10. Variation in triaxial compression strength with fatigue factors under confining stress of 2, 5 MPa.

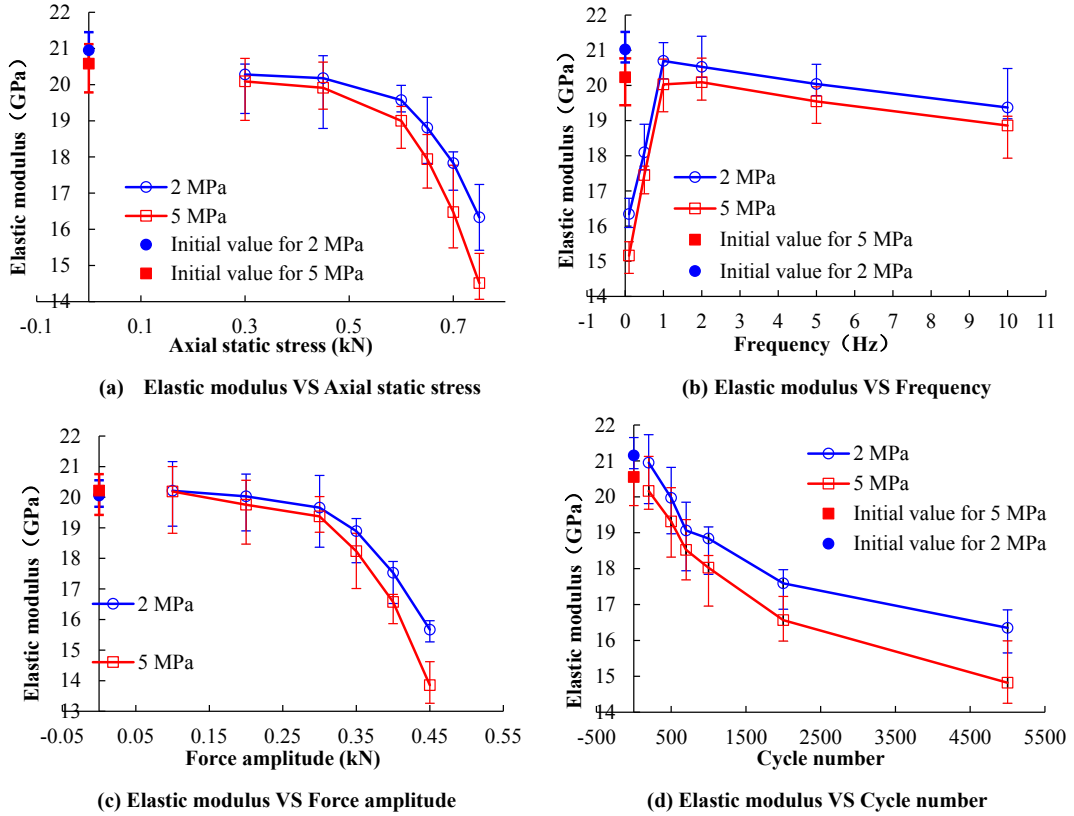

Fig. 11. Variation in elastic modulus with fatigue factors under confining stress of 2, 5 MPa.

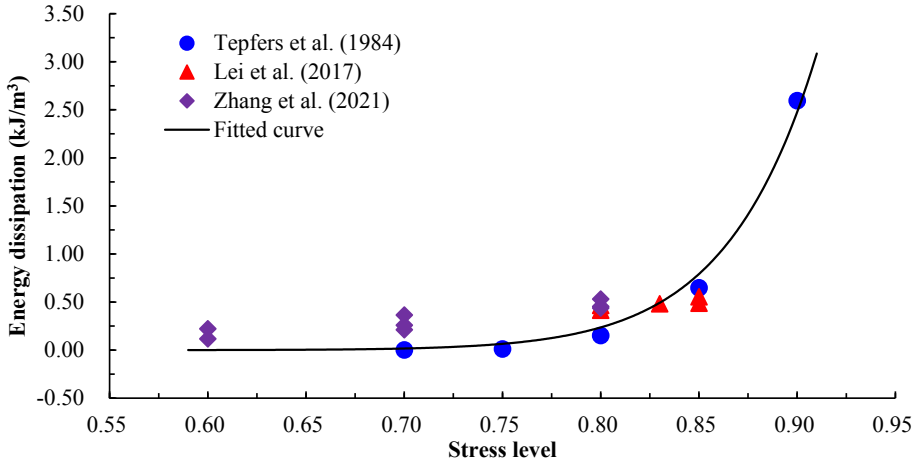

Fig. 12. The relationship between the single-cycle energy dissipation per unit volume and stress level (Zhang et al. [44]).

Table 7
Supplementary data.

Confining stress	Fatigue factor	Supplementary data
2 (in MPa)	Maximum Axial Force	$S_{max}/TCS_2 = 1$, $D_2 = 1.0$
	Cycle number	$N = 0$, $D_2 = 0$
5 (in MPa)	Maximum Axial Force	$S_{max}/TCS_5 = 1$, $D_5 = 1.0$
	Cycle number	$N = 0$, $D_5 = 0$

5.2. Establishment of empirical prediction model for mechanical properties and permeability performance

Furthermore, the relationship of this damage variable to mechanical parameters (TCS and EM) and permeability are established separately (see Fig. 14), and the equations of the best-fit line and the correlation coefficients are determined for each regression regime. In all of the cases, the linear regression relationships are obtained between damage variable versus TCS, EM, and permeability, and the regression equations and correlation coefficients are also given in Table 9. Regression analysis results indicate that the mechanical parameters (TCS and EM) and

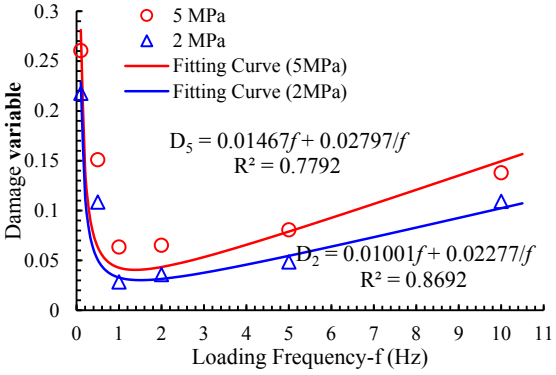

(a) Damage variable VS Loading frequency

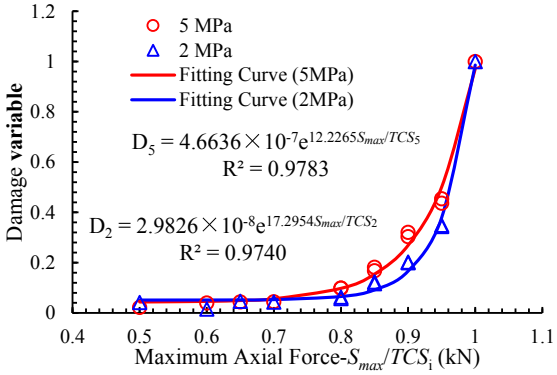

(b) Damage variable VS Maximum axial force

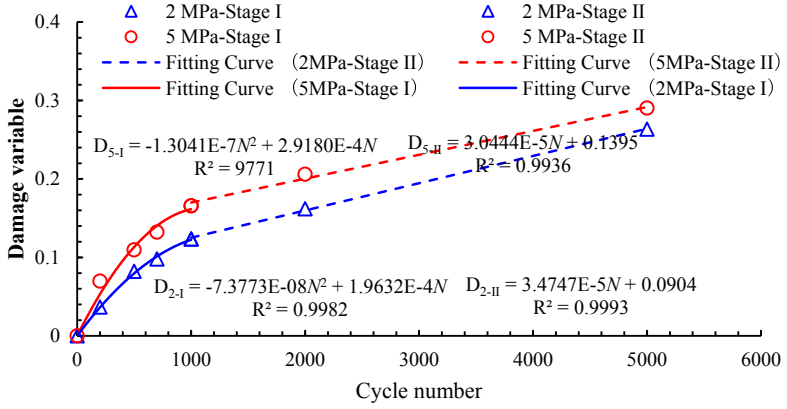

(c) Damage variable VS Cycle number

Fig. 13. Relationships between damage variable and fatigue factors.

Table 8
Regression analysis results.

Confining stress	Parameters to be related	Regression equation	R^2 value
2 (in MPa)	Damage variable –LF (in Hz)	$D_2 = 0.01001f + 0.02277/f$	0.8692
	Damage variable – S_{max}/TCS_2	$D_2 = 2.9826 \times 10^{-8}e^{17.2954Smax/TCS2}$	0.9740
	Damage variable-CN	$D_{2\text{-I}} = -7.3773E{-}08\ N^2 + 1.9632E\text{-}4N$	0.9982
		$D_{2\text{-II}} = 3.4747E{-}5N + 0.0904$	0.9993
5 (in MPa)	Damage variable –LF (in Hz)	$D_5 = 0.01467f + 0.02797/f$	0.7792
	Damage variable–S_{max}/TCS_5	$D_5 = 4.6636 \times 10^{-7}e^{12.2265Smax/TCS5}$	0.9783
	Damage variable-CN	$D_{5\text{-I}} = -1.3041E{-}7N^2 + 2.9180E{-}4N$	0.9771
		$D_{5\text{-II}} = 3.0444E{-}5N + 0.1395$	0.9936

permeability approach the initial value of the intact specimen when the damage variable is zero, which is easy to understand. The error analysis results are shown in Table 10. Thus, the regression equations can be written as a unified model, please see Equation (3).

$$X_i = \eta D + X_{0i} \tag{3}$$

where X_i means that the mechanical parameters (TCS and EM) and permeability of concrete subjected to fatigue disturbance under confining stress of i MPa; η is the slope of regression curve, which will be changed for different parameters; D is the damage variable; X_{0i} means that the mechanical parameters (TCS and EM) and permeability of intact concrete under confining stress of i MPa.

In addition, it is interesting that the slopes of the regression curve (η) of TCS and EM are the same for the concrete subjected to fatigue loading under different confining stress (Fig. 13(a) and (b)), which indicates that the slope of the regression curve (η) is not related to confining stress. However, the slopes of the regression curve of permeability are different. This is caused by the different confining stresses being applied during different stages of permeability measurement, please see Fig. 15. Therefore, a conclusion here can be inferred that the slope of the regression curve is not related to confining stress under consistent confining stress conditions such as Fig. 15(a). Furthermore, based on the evolution equation of permeability under the consistent confining stress of 2 MPa, $K_2 = 6.8058D + K_{02}$, the evolution model of permeability under the consistent confining stress of 5 MPa could be predicted as $K_{5\text{-pre}} = 6.8058D + K_{05}$. Here, $K_{05} = 1.4204 \times 10^{-18}$ m^2. Thus, the

Table 9
Regression analysis results.

Confining stress	Parameters to be related	Regression equation	R^2 value
2 (in MPa)	TCS (in MPa)–D	$TCS_2 = -46.835D + 77.53$	0.8570
	EM (in GPa)–D	$EM_2 = -15.352D + 20.651$	0.8570
	Permeability (in $10^{-18}m^2$)-D	$K_2 = 6.8058D + 2.7507$	0.6066
5 (in MPa)	UCS (in MPa)–D	$TCS_5 = -45.731D + 110.19$	0.6547
	EM (in GPa)–D	$EM_5 = -15.228D + 20.556$	0.8835
	Permeability (in $10^{-18}m^2$)- D	$K_5 = 14.673D + 2.8907$	0.6445

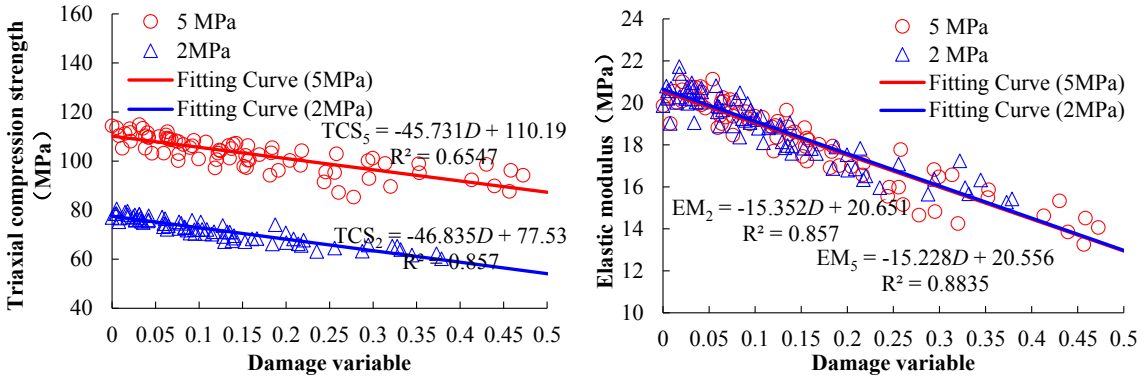

(a) Triaxial compression strength VS Damage variable

(b) Elastic modulus VS Damage variable

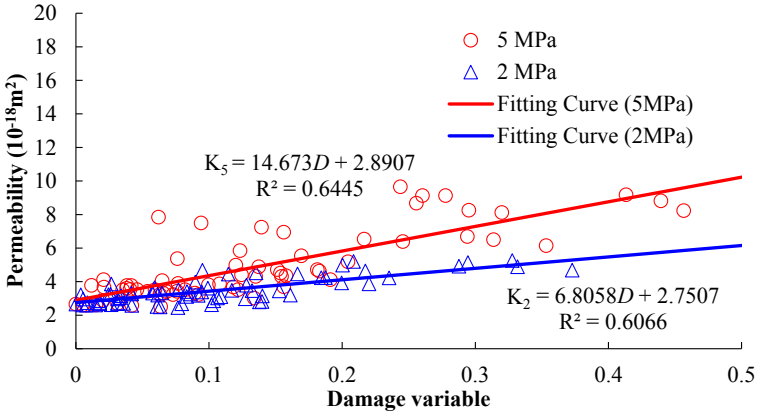

(c) Elastic modulus VS Damage variable

Fig. 14. Correlations between damage variable and physical–mechanical properties.

Table 10
Error analysis results.

Confining stress	Regression equation	D = 0	Initial value	Error (%)
2 (in MPa)	$TCS_2 = -46.835D + 77.53$	$TCS_2 = 77.53$ (in MPa)	77.66 (in MPa)	−0.17
	$EM_2 = -15.352D + 20.651$	$EM_2 = 20.651$ (in GPa)	20.06 (in GPa)	2.95
	$K_2 = 6.8058D + 2.7507$	$K_2 = 2.7507$ (in $10^{-18}m^2$)	2.63 (in $10^{-18}m^2$)	4.59
5 (in MPa)	$TCS_5 = -45.731D + 110.19$	$TCS_5 = 110.19$ (in MPa)	112.36 (in MPa)	−1.93
	$EM_5 = -15.228D + 20.556$	$EM_5 = 20.556$ (in GPa)	20.10 (in GPa)	2.27
	$K_5 = 14.673D + 2.8907$	$K_5 = 2.8907$ (in $10^{-18}m^2$)	2.71 (in $10^{-18}m^2$)	6.67

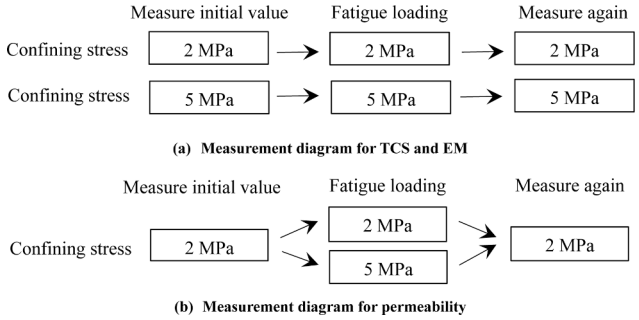

Fig. 15. The measurement diagram.

Table 11
Empirical prediction model.

Parameters to be related	Regression equation	Coefficient	Sequence of confining stress
TCS (in MPa)–D	$TCS_2 = \beta D + TCS_{02}$	$\beta = -46.238$	2 MPa–2 MPa −2 MPa
	$TCS_5 = \beta D + TCS_{05}$		5 MPa–5 MPa −5 MPa
EM (in GPa)–D	$EM_2 = \gamma D + EM_{02}$	$\gamma = -15.290$	2 MPa–2 MPa −2 MPa
	$EM_5 = \gamma D + EM_{05}$		5 MPa–5 MPa −5 MPa
Permeability (in $10^{-18}m^2$)-D	$K_2 = \zeta D + K_{02}$	$\zeta = 6.8058$	2 MPa–2 MPa −2 MPa
	$K_{5\text{-predicted}} = \zeta D + K_{05}$		5 MPa–5 MPa −5 MPa
	$K_5 = \theta D + K_{05}$	$\theta = 14.673$	2 MPa–5 MPa −2 MPa

empirical prediction model of mechanical parameters (TCS and EM) and permeability can be established, please see Table 11, where the sequence of confining stress means that the confining stress is applied in different experimental stages as shown in Fig. 15.

Therefore, the loss of bearing capacity and permeability performance caused by fatigue loading in the design of any concrete construction could be quantitatively predicted under different confining stress, with reference to the fatigue damage model and empirical prediction model in Tables 8 and 11, based on the measurement of S-wave velocity that is an easy and simple task in the site. However, it should be pointed out that the empirical prediction model is established based on existing experimental data, thus, its applicability needs to be discussed for other test conditions.

6. Conclusion

In this work, the coupled 3D fatigue-static loading experiment is carried out, investigation on the post-fatigue characteristics of high-strength concrete including P-wave velocity, S-wave velocity, porosity, gas permeability, triaxial compression strength, and elastic modulus, and establishment of fatigue damage model considering various fatigue factors (axial static stress, loading frequency, force amplitude, cycle number and confining stress) and empirical prediction model for mechanical properties and permeability performance, the following conclusions can be drawn:

(1) The 3D fatigue loading leads to the weakening of mechanical properties, delay of wave propagation, and increase of the transport paths of high-strength concrete. Thus, the triaxial compression strength, elastic modulus, P-wave velocity, and S-wave velocity are decreased, whilst the permeability and porosity are increased.
(2) Damage caused by axial fatigue loading under the confining stress of 5 MPa is greater than that of 2 MPa. This implies that the promotion effect of axial fatigue load on damage is larger than the restriction of confining stress, that is, the damage has a higher sensitivity to the axial loads compared to confining stress during 3D fatigue loading.
(3) Discussion of the influence of different fatigue factors on the weakening characteristics of high-strength concrete, and analysis of their weakening mechanism. With the increase of axial static stress and force amplitude, there is an obvious stress threshold, where the physico-mechanical characteristics of high-strength concrete are rapidly weakened due to the energy dissipation caused by crack growth rises increasingly after exceeding the maximum stress level of 80% TCS_2/TCS_5. Secondly, a noticeable decrease-increase transition characteristic is exhibited for weakening effect with increasing frequency, where the weakening effect is decreased from 0.1 Hz to 1.0 Hz due to the reduction of creep damage accumulation, whilst the self-heating effect enhances the weakening effect from 1.0 Hz to 10.0 Hz. However, it is interesting that the frequency turning point of the weakening effect is advanced under 3D fatigue loading compared with 1D fatigue loading, from 4.0 ~ 15.0 Hz to 1.0 Hz. Finally, the weakening effect shows an obvious two-stage evolution with increasing cycle number. At the low-cycle level, a nonlinear variation is exhibited due to the growth of cracks with strong randomness in the initiation stage, whilst a good linear weakening effect is given owing to the growth of cracks is in the stable propagation stage at the high-cycle level.
(4) Based on the S-wave velocity that is an easy and simple task in the site, the fatigue damage models considering fatigue factors such as axial static stress, loading frequency, force amplitude, and cycle number are proposed under different confining stress. Furthermore, the empirical prediction models of this damage variable to mechanical parameters (triaxial compression strength and elastic modulus) and permeability of high-strength concrete subjected to 3D fatigue loading are established. Therefore, the loss of bearing capacity and permeability performance caused by fatigue loading in the design of any concrete construction could be quantitatively predicted with reference to the fatigue damage model and the empirical prediction model.

The testing results in this context could facilitate our understanding of post-fatigue characteristics of high-strength concrete subjected to 3D fatigue loading, and provide a reference for predicting the loss of bearing capacity and permeability performance caused by fatigue loading in the design of any concrete construction for any designer.

CRediT authorship contribution statement

Fujian Yang: Writing – original draft, Methodology, Investigation, Formal analysis. **Dawei Hu:** Conceptualization, Methodology, Writing -

review & editing, Supervision. **Hui Zhou:** Writing - review & editing, Resources, Formal analysis. **Mao Teng:** Validation, Data curation, Visualization. **Meili Lan:** Writing - review & editing, Validation. **Qi Teng:** Data curation, Visualization.

Declaration of Competing Interest

The authors declare that they have no known competing financial interests or personal relationships that could have appeared to influence the work reported in this paper.

Acknowledgments

The financial was supported by the National Key Research and Development Program of China (Grant Nos. 2018YFC0809600 and 2018YFC0809601; 2019YFC0605103 and 2019YFC0605104), National Natural Science Foundation of China (Grant No. 51779252), and Geological Survey Project of China Geological Survey (Grant No. DD20190128).

References

[1] Y. Guo, X. Chen, X. Li, et al., Experimental study on fracture behavior of three-graded concrete under cyclic loading after initial static loading, Theor. Appl. Fract. Mech. 103 (2019) 102272, https://doi.org/10.1016/j.tafmec.2019.102272.
[2] Q. Li, B. Huang, S. Xu, B. Zhou, R.C. Yu, Compressive fatigue damage and failure mechanism of fiber reinforced cementitious material with high ductility, Cem. Concr. Res. 90 (2016) 174–183, https://doi.org/10.1016/j.cemconres.2016.09.019.
[3] A. Baktheer, J. Hegger, R. Chudoba, Enhanced assessment rule for concrete fatigue under compression considering the nonlinear effect of loading sequence, Int. J. Fatigue 126 (2019) 130–142, https://doi.org/10.1016/j.ijfatigue.2019.04.027.
[4] J.Z. Li, T.B. Peng, Y. Xu, Damage investigation of girder bridges under the Wenchuan earthquake and corresponding seismic design recommendations, Earthq. Eng. Eng. Vib. 7 (4) (2008) 337–344, https://doi.org/10.1007/s11803-008-1005-6.
[5] J. Xiao, L. Hong, Z. Yang, Fatigue behavior of recycled aggregate concrete under compression and bending cyclic loadings, Constr. Build. Mater. 38 (2013) 681–688, https://doi.org/10.1016/j.conbuildmat.2012.09.024.
[6] J. Xiao, Q. Liu, Y.C. Wu, Numerical and experimental studies on fracture process of recycled concrete. Fatigue Fract. Eng. M. 35(8), 801–808. 10.1111/j.1460-2695.2012.01673.x.
[7] K. Keerthana, J.M. Chandra Kishen, Micromechanics of fracture and failure in concrete under monotonic and fatigue loadings, Mech. Mater. 148 (2020) 103490, https://doi.org/10.1016/j.mechmat.2020.103490.
[8] J. Fan, D. Jiang, J. Chen, W. Liu, W. Tiedeu Ngaha, J. Chen, Fatigue performance of ordinary concrete under discontinuous cyclic loading, Constr. Build. Mater. 166 (2018) 974–981, https://doi.org/10.1016/j.conbuildmat.2018.01.115.
[9] Y. Du, J. Wei, J. Yuan, et al., Experimental research on fatigue behavior of prestressed concrete beams under constant-amplitude and variable-amplitude fatigue loading, Constr. Build. Mater. 259 (2020) 119852, https://doi.org/10.1016/j.conbuildmat.2020.119852.
[10] I.N. Yadav, K.B. Thapa, Fatigue damage model of concrete materials, Theor. Appl. Fract. Mech. 108 (2020) 102578, https://doi.org/10.1016/j.tafmec.2020.102578.
[11] K. Keerthana, J.M. Chandra Kishen, Non-local damage model for concrete under variable amplitude loading, ICF 2017-14th Int. Conf. Fract. 2 (2017) 476-477.
[12] K. Keerthana, J.M. Chandra Kishen, An experimental and analytical study on fatigue damage in concrete under variable amplitude loading, Int. J. Fatigue 111 (2018) 278–288, https://doi.org/10.1016/j.ijfatigue.2018.02.014.
[13] X. Chen, D. Shi, N. Shen, et al., Experimental study and analytical modeling on fatigue properties of pervious concrete made with natural and recycled aggregates, Int. J. Concr. Struct. Mater. 13 (2019) 10, https://doi.org/10.1186/s40069-018-0305-0.
[14] X. Chen, D. Shi, N. Shen, et al., Correction to: experimental study and analytical modeling on fatigue properties of pervious concrete made with natural and recycled aggregates, Int. J. Concr. Struct. Mater. 15 (2021) 10, https://doi.org/10.1186/s40069-020-00454-5.
[15] L.B. Gao, C.T.T. Hsu, Fatigue of concrete under uniaxial compression cyclic loading, ACI Mater. J. 95 (5) (1998) 575–581, https://doi.org/10.1016/S1359-6462(98)00243-7.
[16] Z. Tang, W. Li, V.W. Tam, et al., Mechanical behaviors of cfrp-confined sustainable geopolymeric recycled aggregate concrete under static and cyclic compression, Compos. Struct. 252 (2020) 112750, https://doi.org/10.1016/j.compstruct.2020.112750.
[17] F. Yang, D. Hu, H. Zhou, J. Lu, Physico-mechanical behaviors of granite under coupled static and dynamic cyclic loadings, Rock Mech. Rock Eng. 53 (5) (2020) 2157–2173, https://doi.org/10.1007/s00603-019-02040-y.
[18] M.K. Lee, B.I.G. Barr, An overview of the fatigue behaviour of plain and fibre reinforced concrete, Cem. Concr. Comp. 26 (4) (2004) 299–305, https://doi.org/10.1016/S0958-9465(02)00139-7.
[19] K. Aas-Jakobsen, R. Lenschow, Behaviour of reinforced concrete subjected to fatigue loading, ACI J. 70 (1973) 199–206.
[20] A.E. Naaman, H. Hammoud, Fatigue characteristics of high performance fiber-reinforced concrete, Cem. Concr. Comp. 20 (5) (1998) 353–363, https://doi.org/10.1016/S0958-9465(98)00004-3.
[21] Y.J. Kim, P.J. Heffernan, Fatigue behavior of externally strengthened concrete beams with fiber-reinforced polymers: state of the art, J. Compos. Constr. 12 (3) (2008) 246–256, https://doi.org/10.1061/(ASCE)1090-0268(2008)12:3(246).
[22] B.G. Charalambidi, T.C. Rousakis, A.I. Karabinis, Analysis of the fatigue behavior of reinforced concrete beams strengthened in flexure with fiber reinforced polymer laminates, Compos. Part B-Eng. 96 (2016) 69–78, https://doi.org/10.1016/j.compositesb.2016.04.014.
[23] M. Steffen, M. Viktor, Fatigue behaviour of strain-hardening cement-based composites (SHCC), Cem. Concr. Res. 92 (2017) 75–83, https://doi.org/10.1016/j.cemconres.2016.11.003.
[24] R. Tepfers, T. Kutti, Fatigue strength of plain, ordinary, and lightweight concrete, ACI J. 76 (5) (1979) 635–652.
[25] T.T.C. Hsu, Fatigue of plain concrete, ACI J. 78 (4) (1981) 292–305, https://doi.org/10.1016/0022-3115(81)90580-8.
[26] J. Holmen, Fatigue of concrete by constant and variable amplitude loading, Fatigue Concr. Struct. 75 (1982) 71–110.
[27] J. Qiu, E.H. Yang, Micromechanics-based investigation of fatigue deterioration of engineered cementitious composite (ECC), Cem. Concr. Res. 95 (2017) 65–74, https://doi.org/10.1016/j.cemconres.2017.02.029.
[28] Z. Ding, D.-C. Feng, X. Ren, J. Wang, Physically based constitutive modeling of concrete fatigue and practical numerical method for cyclic loading simulation, Eng. Failure Anal. 101 (2019) 230–242, https://doi.org/10.1016/j.engfailanal.2019.03.020.
[29] S. Khalilpour, E. Baniasad, M. Dehestani, A review on concrete fracture energy and effective parameters, Cem. Concr. Res. 120 (2019) 294–321, https://doi.org/10.1016/j.cemconres.2019.03.013.
[30] S. Raya, C.C. Jeshnaa, N. Guptab, Fatigue life assessment of concrete members under variable amplitude loading: an analytical approach, Eng. Fract. Mech. 223 (2020) 106735, https://doi.org/10.1016/j.engfracmech.2019.106735.
[31] P. Paris, F. Erdogan, Reviews of a critical analysis of crack propagation laws, J. Basic Eng. 85 (4) (1963) 528–534, https://doi.org/10.1115/1.3656900.
[32] Z.P. Bažant, K. Xu, Size effect in fatigue fracture of concrete, ACI Mater. J. 88 (4) (1991) 390–399.
[33] Z. Bažant, W.F. Schell, Fatigue fracture of high-strength concrete and size effect, ACI Mater. J. 90 (5) (1993) 472–478.
[34] V. Slowik, G.A. Plizzari, V.E. Saouma, Fracture of concrete under variable amplitude fatigue loading, ACI Mater. J. 93 (3) (1996) 272–283, https://doi.org/10.1016/0040-6090(95)08175-5.
[35] A. Carpinteri, A. Spagnoli, S. Vantadori, A multifractal analysis of fatigue crack growth and its application to concrete, Eng. Fract. Mech. 77 (6) (2010) 974–984, https://doi.org/10.1016/j.engfracmech.2010.01.019.
[36] A. Alliche, Damage model for fatigue loading of concrete, Int. J. Fatigue 26 (9) (2004) 915–921, https://doi.org/10.1016/j.ijfatigue.2004.02.006.
[37] G.D. Nguyen, A thermodynamic approach to non-local damage modelling of concrete, Int. J. Solids Struct. 45 (7) (2008) 1918–1934, https://doi.org/10.1016/j.ijsolstr.2007.11.001.
[38] Y.P. Wang, Physical stochastic damage model for concrete subjected to fatigue loading, Int. J. Fatigue 121 (2019) 191–196, https://doi.org/10.1016/j.ijfatigue.2018.12.023.
[39] K. Kawashima, G.A. Macrae, J.I. Hoshikuma, et al., Residual displacement response spectrum, Int. J. Solids Struct. 124 (5) (1998) 523–530, https://doi.org/10.1061/(ASCE)0733-9445(1998)124:5(523).
[40] S. Li, T.Y. Zhao, M.S. Alam, et al., Probabilistic seismic vulnerability and loss assessment of a seismic resistance bridge system with post-tensioning precast segmental ultra-high performance concrete bridge columns, Eng. Struct. 225 (2020) 111321, https://doi.org/10.1016/j.engstruct.2020.111321.
[41] F. Yang, D. Hu, H. Zhou, et al., Physical and mechanical properties of granite after dynamic disturbance, Chinese J. Rock Mech. Eng. 37 (6) (2018) 1459–1467. 10.13722/j.cnki.jrme.2018.0068.
[42] C. Jiang, X. Gu, Q. Huang, W. Zhang, Deformation of concrete under high-cycle fatigue loads in uniaxial and eccentric compression, Constr. Build. Mater. 141 (2017) 379–392, https://doi.org/10.1016/j.conbuildmat.2017.03.023.
[43] J. Wu, J. Xu, B. Diao, et al., Impacts of reinforcement ratio and fatigue load level on the chloride ingress and service life estimating of fatigue loaded reinforced concrete (RC) beams, Constr. Build. Mater. 266 (2021) 120999, https://doi.org/10.1016/j.conbuildmat.2020.120999.
[44] Q. Zhang, L. Wang, Investigation of stress level on fatigue performance of plain concrete based on energy dissipation method, Constr. Build. Mater. 269 (2021) 121287, https://doi.org/10.1016/j.conbuildmat.2020.121287.
[45] B. Sun, Z. Xu, An efficient numerical method for meso-scopic fatigue damage analysis of heterogeneous concrete, Constr. Build. Mater. 278 (2021) 122395, https://doi.org/10.1016/j.conbuildmat.2021.122395.
[46] L. Basheer, J. Kropp, D. Cleland, Assessment of the durability of concrete from its permeation properties: a review, Constr. Build. Mater. 15 (2–3) (2001) 93–103, https://doi.org/10.1016/S0950-0618(00)00058-1.
[47] W. Xue, X. Liu, W. Jing, et al., Experimental study and mechanism analysis of permeability sensitivity of mechanically damaged concrete to confining pressure,

Cem. Concr. Res. 134 (2020) 106073, https://doi.org/10.1016/j.cemconres.2020.106073.
[48] W. Xue, L. Shen, W. Jing, et al., Permeability evolution and mechanism of thermally damaged basalt fiber-reinforced concrete under effective stress, Constr. Build. Mater. 251 (2020) 119077, https://doi.org/10.1016/j.conbuildmat.2020.119077.
[49] H. Tu, H. Zhou, J. Lu, et al., Elastoplastic coupling analysis of high-strength concrete based on tests and the mohr-coulomb criterion, Constr. Build. Mater. 255 (2020) 119375, https://doi.org/10.1016/j.conbuildmat.2020.119375.
[50] Standard for Test and Evaluation of Concrete Compression Strength, 2010. GB50107-2010.
[51] Technical Specification for Strength Testing of High Strength Concrete, 2013, JGJ/T 294-2013.
[52] Z.T. Bieniawski, M.J. Bernede, Suggested methods for determining the uniaxial compressive strength and deformability of rock materials, Int. J. Rock Mech. Min. Geomech. Abs. 16 (2) (1979) 138–140, https://doi.org/10.1016/0148-9062(79)91451-7.
[53] M. Gong, I. Smith, Effect of waveform and loading sequence on low-cycle compressive fatigue life of spruce, J. Mater. Civ. Eng. 15 (1) (2003) 93–99, https://doi.org/10.1061/(ASCE)0899-1561(2003)15:1(93).
[54] D. Hu, H. Zhou, F. Zhang, et al., Evolution of poroelastic properties and permeability in damaged sandstone, Int. J. Rock Mech. Min. 47 (6) (2010) 962–973, https://doi.org/10.1016/j.ijrmms.2010.06.007.
[55] Z. Liu, J. Shao, D. Hu, et al., Gas permeability evolution with deformation and cracking process in a white marble under compression, Transp. Porous Media 111 (2) (2016) 441–455, https://doi.org/10.1007/s11242-015-0603-9.
[56] L. Skarzynski, I. Marzec, J. Tejchman, Fracture evolution in concrete compressive fatigue experiments based on X-ray micro-CT images, Int. J. Fatigue 122 (2019) 256–272, https://doi.org/10.1016/j.ijfatigue.2019.02.002.
[57] X. Chen, J. Bu, X. Fan, J. Lu, L. Xu, Effect of loading frequency and stress level on low cycle fatigue behavior of plain concrete in direct tension, Constr. Build. Mater. 133 (2017) 367–375, https://doi.org/10.1016/j.conbuildmat.2016.12.085.
[58] R. Tepfers, B. Hedberg, G. Szczekocki, Absorption of energy in fatigue loading of plain concrete, Mater. Struct. 17 (1) (1984) 59–64, https://doi.org/10.1007/BF02474058.
[59] D. Lei, P. Zhang, J. He, P. Bai, F. Zhu, Fatigue life prediction method of concrete based on energy dissipation, Constr. Build. Mater. 145 (2017) 419–425, https://doi.org/10.1016/j.conbuildmat.2017.04.030.
[60] J.W. Murdock, A critical review of research on fatigue of plain concrete, PhD. Thesis University Illinois USA, 1965.
[61] A.C.I. Committee, 215, Considerations for design of concrete structures subjected to fatigue loading, ACI J. 71 (1974) 97–121.
[62] A. Jansen, Research to fatigue behavior of topping on prefabricated concrete girders, PhD. Thesis Delft University Technology Netherlands, 1996.
[63] C. Thomas, J. Sainz-Aja, J. Setien, et al., Resonance fatigue testing on high-strength self-compacting concrete, J. Build Eng. 35 (2020) 102057, https://doi.org/10.1016/j.jobe.2020.102057.
[64] J. Sainz-Aja, C. Thomas, I. Carrascal, et al., Fast fatigue method for self-compacting recycled aggregate concrete characterization, J. Cleaner Prod. 277 (2020) 123263, https://doi.org/10.1016/j.jclepro.2020.123263.
[65] M. Eftekhari, A. Fatemi, On the strengthening effect of increasing cycling frequency on fatigue behavior of some polymers and their composites: experiments and modeling, Int. J. Fatigue 87 (2016) 153–166, https://doi.org/10.1016/j.ijfatigue.2016.01.014.
[66] A. Fatemi, L. Yang, Cumulative fatigue damage and life prediction theories: a survey of the state of the art for homogeneous materials, Int. J. Fatigue 20 (1) (1998) 9–34, https://doi.org/10.1016/S0142-1123(97)00081-9.
[67] B.H. Oh, Cumulative damage theory of concrete under variable-amplitude fatigue loadings, ACI Mater. J. 88 (1) (1991) 41–48, https://doi.org/10.1061/(ASCE)0733-9445(1991)117:12(3831.2).
[68] B.F. Langer, Fatigue failure from stress cycles of varying amplitude, J. Appl. Mech. 59 (1937) A160–A162.
[69] H.J. Grover, An observation concerning the cycle ratio in cumulative damage, Fatigue Aircr. Struct. 274 (1960) 120–124, https://doi.org/10.1520/STP45928S.
[70] S.S. Manson, Interfaces between fatigue, creep, and fracture, Int. J. Fract. Mech. 2 (1) (1966) 327–363, https://doi.org/10.1007/BF00698478.
[71] S.S. Manson, J.C. Freche, S.R. Ensign, Application of a double linear damage rule to cumulative fatigue, Fatigue Crack Propag. 415 (1967) 384–412.
[72] C.D. Martin "The strength of massive Lac du Bonnet granite around underground openings" PhD. Thesis University Manitoba Canada, 1993.
[73] C.D. Martin, N.A. Chandler, The progressive fracture of lac du bonnet granite, Int. J. Rock Mech. Min. Geomech. Abs. 31 (6) (1994) 643–659, https://doi.org/10.1016/0148-9062(94)90005-1.
[74] E. Eberhardt, D. Stead, B. Stimpson, Identifying crack initiation and propagation thresholds in brittle rock, Can. Geotech. J. 35 (2) (1998) 222–233, https://doi.org/10.1139/cgj-35-2-222.
[75] M. Khandelwal, Correlating p-wave velocity with the physico-mechanical properties of different rocks, Pure Appl. Geophys. 170 (4) (2013) 507–514, https://doi.org/10.1007/s00024-012-0556-7.
[76] J.Q. Xiao, D.X. Ding, F.L. Jiang, et al., Fatigue damage variable and evolution of rock subjected to cyclic loading, Int. J. Rock Mech. Min. 47 (3) (2010) 461–468, https://doi.org/10.1016/j.ijrmms.2009.11.003.